http://dx.doi.org/10.5935/0103-5053.20150283

J. Braz. Chem. Soc., Vol. 27, No. 2, 363-371, 2016.
Printed in Brazil - ©2016 Sociedade Brasileira de Química
0103 - 5053 $6.00+0.00

Article

Cellulose Nanocrystals Assembled on the Fe_3O_4 Surface as Precursor to Prepare Interfaced C/Fe_3O_4 Composites for the Oxidation of Aqueous Sulfide

Igor T. Cunha,[a] Ivo F. Teixeira,[b] João P. Mesquita,[c] José D. Ardisson,[d] Ildefonso Binatti,[e] Fabiano V. Pereira[a] and Rochel M. Lago[,a]*

[a]*Departamento de Química, Universidade Federal de Minas Gerais, 31270-901 Belo Horizonte-MG, Brazil*

[b]*Department of Chemistry, University of Oxford, OX12JA Oxford, United Kingdom*

[c]*Departamento de Química, Campus II, Universidade Federal dos Vales do Jequitinhonha e Mucuri, 39100-000 Diamantina-MG, Brazil*

[d]*Laboratório de Física Aplicada, CDTN, 31270-901 Belo Horizonte-MG, Brazil*

[e]*Centro Federal de Educação Tecnológica de Minas Gerais, 30421-169 Belo Horizonte-MG, Brazil*

In this work, composites based on carbon (1, 10 and 20 wt.%) interfaced with Fe_3O_4 (magnetite) have been studied as catalysts for the oxidation of aqueous sulfide. The composites were prepared by assembling cellulose nanocrystals surrounding Fe_3O_4 followed by a controlled thermal decomposition at 400, 600 and 800 °C. Mössbauer, X-ray diffractometry (XRD), Raman, thermogravimetry (TG), elemental analysis CHN, scanning electron microscopy (SEM/EDS), Fourier transform infrared spectroscopy (FTIR) and potentiometric titration indicated that at 400 and 600 °C the cellulose nanocrystals decompose to different carbon forms, i.e., films, filaments and particles attached to the Fe_3O_4 crystals. At higher temperature, i.e., 800 °C, this carbon on the magnetite surface further reacted to produce Fe^0. UV-Vis, Raman and electrospray ionization mass spectrometry (ESI-MS) measurements showed that these composites catalyze the oxidation of aqueous sulfide to convert S^{2-}_{aq} to polysulfides S_n^{2-} (where n = 2-9) and also oxygen containing polysulfides HOS_n^-. Simple kinetic experiments showed very low sulfide oxidation activities for pure Fe_3O_4 and pure carbon. On the other hand, the composites, especially with 10% C obtained at 600 °C, were remarkably active. These results are discussed in terms of a possible participation of oxygen based redox groups present on the carbon surface and an electron transfer from the carbon to the Fe_3O_4 phase.

Keywords: magnetite, cellulose nanocrystal, whisker, sulfide oxidation, polysulfide

Introduction

Sulfide in industry is commonly found as H_2S and for a variety of reasons, e.g., aesthetics (odor control),[1] health (toxicity), ecological (oxygen depletion in receiving waters),[2,3] and economic (corrosion of equipment and infrastructure),[4] there is a considerable interest to eliminate sulfide from wastewaters.[5]

The removal of hydrogen sulfide has been studied by different processes, among them sulfide oxidation is one of the most explored. Catalytic oxidation of H_2S using air is applied using different catalysts, i.e., vanadium,[6] iron oxides.[7] The oxidation of H_2S is also being investigated using hydrogen peroxide and Mo^{VI} based catalysts.[8] Regarding the oxidation of aqueous sulfide, studies have been exploring the utilization of activated carbons[9] and modified carbon based materials such as graphite and graphene.[10]

Microorganisms showed potential to oxidize sulfide into different sulfur-containing species, e.g., elemental sulfur, polysulfides, thiosulfate, thionates and sulfate in aqueous medium.[11-13] Some of these bacteria were *Wolinella succinogenes*,[14] *Rhodobacter capsulatus*, *Pelodictyon luteolum*, and *Chlorobium*.[15] The ability of these microorganisms to perform sulfide oxidation has been associated with the presence of the sulfide-quinone

*e-mail: rochel@ufmg.br

reductase enzyme.[16,17] The activity of this enzyme is due to the presence of quinone redox groups and a facile electron transportation system.

Based on these features a new family of more active and robust catalysts was developed using different forms of carbon such as activated carbon,[9] graphite and graphene.[10] These carbons possess relatively high area and chemically stable surface, which can be functionalized with redox quinone groups. Moreover, the graphene like structures present in these carbons play an important role due to the electron conduction during sulfide oxidation.[9,10]

It has also been developed active inorganic catalysts based on ferrites MFe_2O_4 (M = Cu, Co) which combines surface redox groups (Cu^{2+}/Cu^{+}, Fe^{3+}/Fe^{2+}, Co^{3+}/Co^{2+})[18] and an electron conducting structure.[18]

In this work, it was developed a novel catalyst based on the combination of carbon structures containing active oxygen surface redox groups interfaced with Fe_3O_4, which is an excellent electron conducting oxide. These composite catalysts have been prepared by the impregnation of cellulose nanocrystals (CNC) on the magnetite surface. Some of the potential features of this system are: (*i*) the cellulose nanocrystals should interact well with the Fe_3O_4 surface via H-bonding to produce a good dispersion and interface; (*ii*) the cellulose nanocrystals can assemble around the Fe_3O_4 particles to form sheets, filaments and isolated particles which upon thermal decomposition will produce different forms of carbons, i.e., films, filaments and nanoparticles; (*iii*) these carbon structures should have a high exposed surface with high concentration of oxygen surface groups (Figure 1).

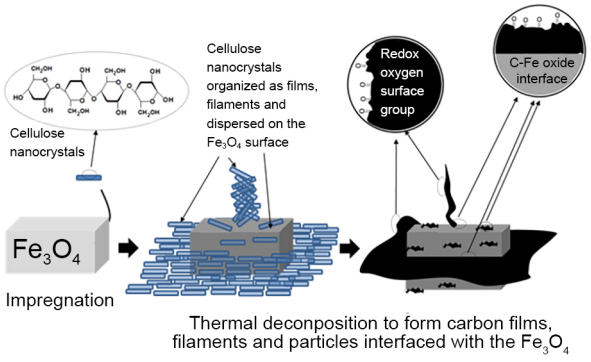

Figure 1. Schematic representation of the preparation of carbon structures by the impregnation and assembling of cellulose nanocrystals in Fe_3O_4 particles followed by thermal decomposition.

This composite has several physico-chemical properties that can potentially promote aqueous sulfide oxidation, especially the carbon structures with high exposed surface, which can act as catalytic sites where quinone redox groups remove electrons from aqueous sulfide ($S^{2-}{}_{aq}$). These electrons can be transferred to Fe_3O_4 that has an excellent redox couple based on Fe^{3+}/Fe^{2+} especially at the octahedral sites of the spinel structure. Moreover, Fe_3O_4 is a conductive solid structure able to disperse the electrons received and finally the magnetic property of these composites allows a facile removal from the reaction medium by a simple magnetic process.

Experimental

The sulfuric acid hydrolysis reaction of eucalyptus kraft wood pulp was performed according to a procedure described elsewhere, with minor modifications.[19,20] Briefly, 10 g of bleached cellulose pulp was added to 160 mL of 64 wt.% sulfuric acid under strong mechanical stirring. Hydrolysis reaction was performed at 55 °C for approximately 25 min.

After hydrolysis, the dispersion was diluted two-fold in water, and the dispersions were washed three times with deionized water by centrifugation. The last washing was conducted using dialysis against deionized water until the dispersion reached a pH of ca. 7. The dispersions were ultrasonicated with an Ultrasonic Processor Cole Parmer CPX750 equipped with a microtip and a stable suspension of CNC was obtained after sonication for approximately 1 min. The obtained aqueous suspension of CNC (ca. 1%, m/v) was freeze-dried to obtain a powder of the cellulose nanoparticles.

The compounds were synthesized by mixing 500 mg of a commercial magnetite (Synth, pretreated under N_2 atmosphere at 900 ºC for 1 h) with different volumes (i.e., 5, 30 and 60 mL) of a cellulose nanocrystals suspension (10 g L^{-1}) followed by evaporation under stirring. The obtained solid was dried in an oven at 80 ºC for 6 h. The samples were then submitted to the following treatment: heating up to 400 ºC at 10 ºC min^{-1} under an atmosphere of H_2/N_2 and after this temperature, the atmosphere was changed to N_2 and the temperature elevated up to 400, 600 or 800 ºC for 1 hour. The catalysts were characterized by X-ray diffraction (Geigerflex Rigaku diffractometer (Cu Kα radiation)), transmission ^{57}Fe Mössbauer (at 25 K on a constant acceleration transducer with a ^{57}Co/Rh source, the Normos least-square fits was employed to calculate the spectral hyperfine parameters), thermogravimetry (TG, DTG-60 Shimadzu in atmosphere of air), Raman (Bruker 100 FT-FRS-Raman, 785 nm, 2 mW laser), Fourier transform infrared spectroscopy (FTIR) spectra of materials were obtained in a Nicolet 380 FT-IR spectrometer (Nicolet, MN), potentiometric titration curves were obtained with a Metrohm 670 automatic titrator, and scanning electron microscopy with energy-dispersive X-ray spectroscopy

SEM/EDS (Jeol JSM 840A and a Quanta 200 ESEM FEG from FEI).

The sulfide oxidation studies were performed using 20 mg of sample in 3 mL of $Na_2S.9H_2O$ (8 g L^{-1}) solution in water. The reaction was carried out at room temperature (25 ºC) under manual homogenization. During the experiments, the reaction solution was collected at different times and the formation of polysulfides was monitored by measuring the absorbance of the aqueous solution at different wavelengths using a Shimadzu UV-2550 Spectrometer. The final solution obtained after oxidation was also characterized by Raman (Bruker 100 FT-FRS-Raman, 785 nm, 2 mW laser) and paper spray mass spectrometry (ThermoElectron LCQFleet operating in the negative ion mode).

Results and Discussion

The catalysts have been prepared by the impregnation of Fe_3O_4 (magnetite) with different cellulose nanocrystal contents. The CNCs/Fe_3O_4 composites were then thermally treated to decompose the CNC to carbon on the Fe_3O_4 surface.[21] The CNC contents were adjusted to produce carbon concentrations of approximately 1, 10 and 20 wt.%. All the composites were treated at 600 ºC and only the composite with 10% carbon was treated at 400, 600 and 800 ºC.

Raman spectra (Supplementary Information) of these samples showed the typical carbon D and G bands, related to defective less organized carbon (at ca. 1300 cm^{-1}) and more organized graphitic carbon (at ca. 1550 cm^{-1}), respectively.

The disorganized structure of the carbon in the surface of the composites is evident by the comparison of the band D (1350 cm^{-1}) and band G (1500-1600 cm^{-1}), where the relative intensity of the band D is higher than the band G. Most of the materials presented bands related to magnetite, but the composite $MW_{600}1$ showed bands of maghemite, likely due to oxidation processes promoted by the laser during Raman analysis.[22] In addition, in the material $MW_{800}10$ the magnetite bands are not present, considering that Fe^0 constitutes most of this material.

FTIR analyses of pure CNC treated at different temperatures (see Supplementary Information section) suggest that up to 400 °C, the obtained carbons have relatively large concentrations of oxygenated functional groups, e.g., intense bands at ca. 1100, 1700 and 3400 cm^{-1} characteristics of νC–O, νC=O and νO–H.[23,24] At temperatures higher than 600 °C these bands strongly decreased in intensity indicating a significant decrease in the concentration of the oxygen containing groups. Potentiometric titration of these carbons (see Supplementary Information section) confirmed that oxygen surface groups with different pKa are decomposed, especially when the treatment temperature increased above 600 ºC.

In Table S1 are shown the concentration of oxygenated functional acid groups determined with potentiometric titration. In general the results are in agreement with the FTIR spectra. The increase in pyrolysis temperature significantly decreases the total acidic functional groups. In addition from 400 ºC occurs the removal of the functional groups with pKa < 5 mainly attributed to the carboxylic functional groups.[25,26]

The C contents were determined by TG (Supplementary Information) in air and also elemental analyses CHN with the obtained values in the range 0.5-1, 9-10 and 20-22 wt.%. These catalysts are named hereon as, e.g., $MW_{800}10$ (M = magnetite, W = whysker, temperature = 800 ºC, 10 wt.% of carbon content).

The samples $MW_{600}1$, $MW_{600}10$ and $MW_{600}20$ showed a similar decomposition pattern, showing a slightly increase in their mass between 300 and 400 ºC due to the oxidation the Fe_3O_4 to γ-Fe_2O_3, and between 400 and 550 ºC a weight loss which is related to the oxidation of carbon.[27] In the sample $MW_{400}10$, the carbon oxidation was observed in lower temperature, between 300 and 400 ºC. On the other hand, for the sample $MW_{800}10$, it was not observed mass loss, possibly because the small amount of remaining carbon, as evidenced by CHN elemental analysis. In addition, the results obtained in the thermogravimetry were also relevant to estimate the amount of carbon in the samples.

The effect of composite with 10% carbon was used to investigate the effect of temperature treated obtained composite were analyzed by Mössbauer spectroscopy at 25 K in order to identify the Fe phases (Figure 2) (see also Supplementary Information section for the hyperfine parameters).

The commercial sample Mt treated at 900 ºC in N_2 showed the typical hyperfine parameters of magnetite, but with the presence of significant amounts of hematite α-Fe_2O_3 contamination (approximately 25% spectral area) due to the natural oxidation of the magnetite in air. For this reason all the materials were prepared by an initial treatment with H_2/N_2 at 400 ºC which reduces all the Fe_2O_3 phases (hematite and maghemite) to magnetite.[28]

The iron phase compositions obtained by Mössbauer are presented in Figures 3 and 4.

The obtained results showed that the treatment at 400 ºC produced 95% Fe_3O_4 and a new phase ca. 5% γ-Fe_2O_3 (maghemite). Several previous works showed that the formation of maghemite typically takes place by the reduction of hematite α-Fe_2O_3 to Fe_3O_4 and/or FeO by H_2, or the volatile reducing molecules (e.g., CO, organics) and carbon, all of them formed during the thermal

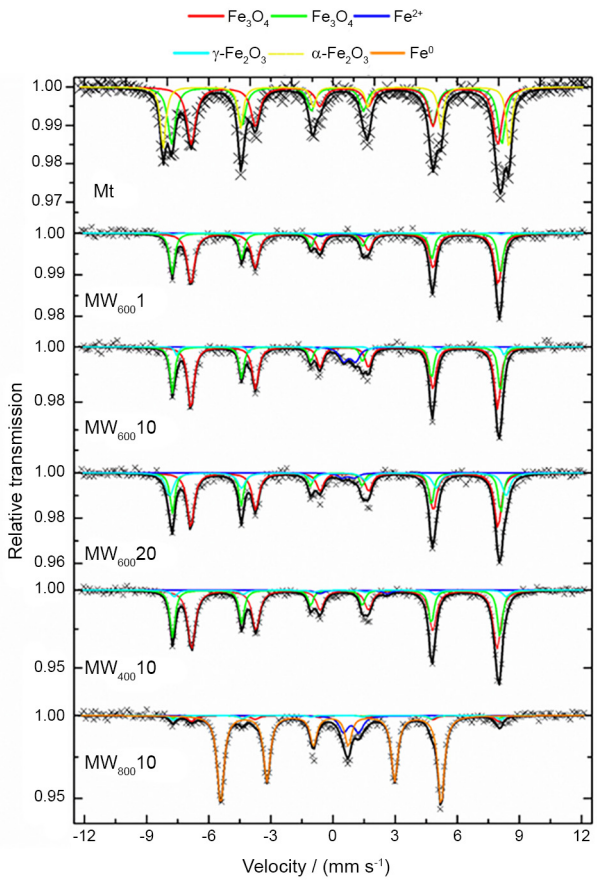

Figure 2. Mössbauer spectra (at 25 K) for Mt (magnetite), $MW_{600}1$, $MW_{400}10$, $MW_{600}10$, $MW_{800}10$ and $MW_{600}20$. In red the octahedral sites and in green the tetrahedral sites.

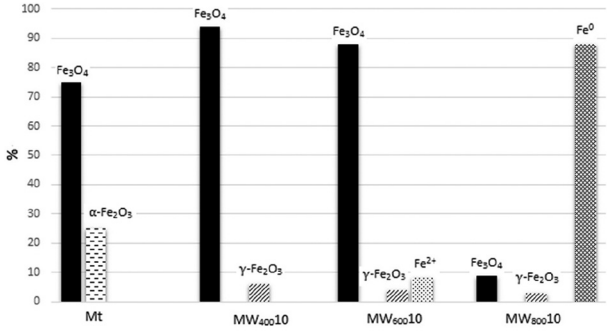

Figure 3. Iron phase compositions determined by Mössbauer spectroscopy for the Fe_3O_4 precursor and for the composites MW with 10% carbon treated at 400, 600 and 800 °C.

decomposition of cellulose.[28-33] The more reactive phases Fe_3O_4 and/or FeO are oxidized by air at room temperature to produce γ-Fe_2O_3.

Upon treatment at 600 °C, a significant concentration of Fe^{2+} is observed likely due to the partial reduction of Fe_3O_4 by superficial carbon or H_2, equation 1.

$$Fe_3O_4 + C/H_2 \rightarrow Fe^{2+} \text{ (e.g., FeO highly dispersed)} + CO_x/H_2O \quad (1)$$

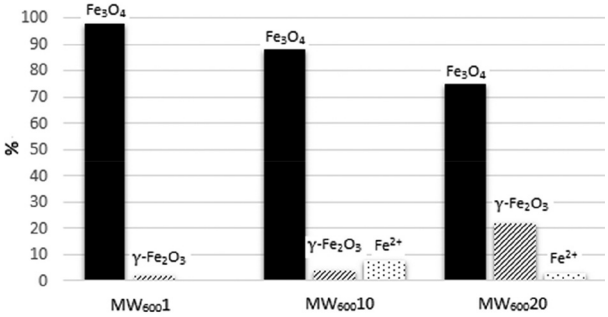

Figure 4. Iron phase compositions determined by Mössbauer spectroscopy for the composites $MW_{600}1$, $MW_{600}10$ and $MW_{600}20$.

At 800 °C, the Fe oxides are further reduced mainly to Fe^0, likely by the simplified reaction with carbon or H_2 (equation 2).

$$Fe_3O_4/FeO + C/H_2 \rightarrow Fe^0 + CO_x/H_2O \quad (2)$$

All these reactions are well known and they have been observed in different systems based on iron oxides with several organic matrices and reducing agents, such as carbon,[28] ethanol,[33] methane,[31] tar pitch,[29] bio-oil,[30] using techniques such as Mössbauer, XRD and magnetization measurementes.[34]

Mössbauer spectra for the samples MW_{600} with 1, 10 and 20% carbon showed that as the carbon content increased in the composite, the relative concentration of the oxidized phase γ-Fe_2O_3 also increased. Although the reason for this effect is not clear, it could be related to the oxidation of Fe_3O_4 by CO_2 and H_2O formed during the decomposition of cellulose. As the cellulose content increased in the samples $MW_{600}1$, $MW_{600}10$ and $MW_{600}20$, the amount of CO_2 and H_2O formed during pyrolysis also increased oxidizing Fe_3O_4 in larger extension as shown in Figure 4.

This is likely related to more extensive reaction of Fe_2O_3. The XRD results confirm the data obtained by Mössbauer spectroscopy (Figure 5).

The prevalence of the spinel phase of Fe_3O_4 (JCPDF 19-629) is observed in the diffraction patterns obtained for the samples Mt, $MW_{600}1$, $MW_{400}10$, $MW_{600}10$ and $MW_{600}20$. The presence of Fe^0 (JCPDF 1-1267) in $MW_{800}10$ sample was also confirmed with the obtained diffraction pattern. The samples presented intense and well-defined peaks, indicating a higher crystallinity.

SEM images showed that the magnetite phase is present as fairly well defined crystal with flat surface (Figure 6). When carbon is present at 1 and especially 10%, the magnetite particles can still be identified, however, completely surrounded by new forms similar to thin films and nanofilaments, likely due to the carbon formed from the cellulose nanocrystals. This morphology

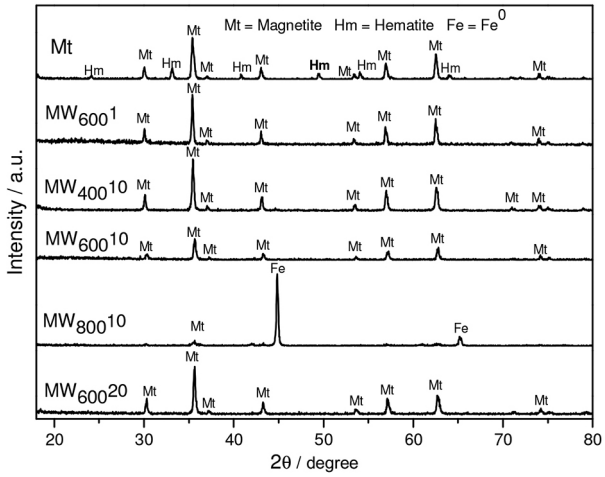

Figure 5. XRD for the samples Mt, and the composites $MW_{600}1$, $MW_{400}10$, $MW_{600}10$, $MW_{800}10$ and $MW_{600}20$.

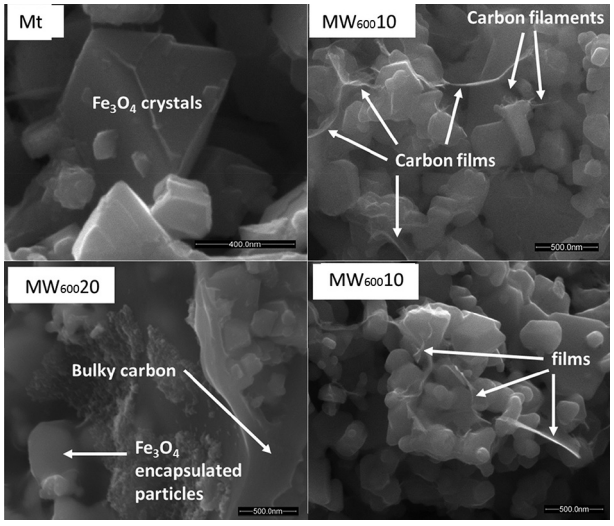

Figure 6. SEM images of pure magnetite and the composites MW_{600} with 10 and 20% carbon.

is typically observed in carbon CNC prepared at 600 °C (Supplementary Information).

On the other hand, at 20% carbon many magnetite particles seem to be encapsulated and the presence of bulky carbon can be clearly observed.

Figure 7 shows that treatments of the composites at 400 and 600 ºC did not cause significant modification of the magnetite particle morphology. On the other hand, treatment at 800 ºC completely changed the magnetite crystals into a more compacted sintered agglomerated particles due to the reduction to Fe^0. EDS spectra obtained for these samples showed the expected signals for Fe, O and C. It is interesting to see that the relatively intensity of the carbon signal strongly decreased for the composite $MW_{800}10$ suggesting that the relative concentration of carbon in this sample decreased. In fact, CHN and TG results showed carbon contents of 9-11% for the composites $MW_{400}10$ and $MW_{600}10$ whereas only < 1% carbon was detected for $MW_{800}10$. This result confirms the Mössbauer and XRD data, which showed that Fe_3O_4 is reduced to Fe^0 by the carbon present in the composite.

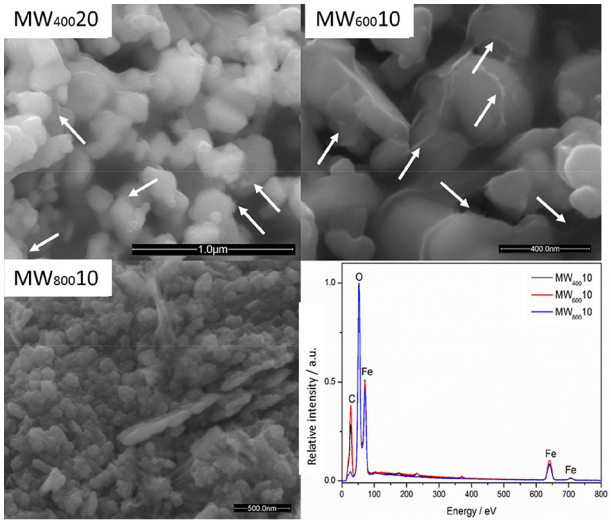

Figure 7. SEM images for the composites $MW_{400}10$, $MW_{600}10$ and $MW_{800}10$ and a comparison of the EDS spectra obtained for each presented image.

The obtained compounds were tested for oxidation of aqueous sulfide. The non-colored sulfide solution became blue in the presence of the catalysts. The UV-Vis spectra (Figure 8) of the sulfide solution gradually showed characteristic bands for small polysulfides species, such as S_2^{2-} (270 nm), S_3^{2-} (300 nm), S_4^{2-} (370 nm),[35] and other polysulfides with chains reaching S_9^{2-}.[36-38] These polysulfides with longer chains are likely responsible for the green/blue color of the solution (detail Figure 8).[39]

These different polysulfides were also identified in a typical Raman spectrum obtained in aqueous medium (Figure 9).

The obtained spectra obtained in aqueous medium showed in general bands with low intensity related to disulfides (S_2^{2-}) at 117 and 164 cm^{-1},[40,41] trisulfides 322 cm^{-1} (S–S–S–H),[42] 578 and 646 cm^{-1}.[43] It was also identified the presence of S_4^{2-} at 78 cm^{-1} [42] and 360 cm^{-1}.[43] Moreover, the band at 78 cm^{-1} may also be related to S_6^{2-} and the bands at 58 and 288 cm^{-1} to S_7^{2-}.[43]

The identification of the products during the oxidation of the sodium sulfide was also carried out using paper spray mass spectrometry (PS-MS) in the negative mode.[44] The spectrum obtained (Figure 10) suggests the presence of polysulfides and other oxygenated sulfur species.

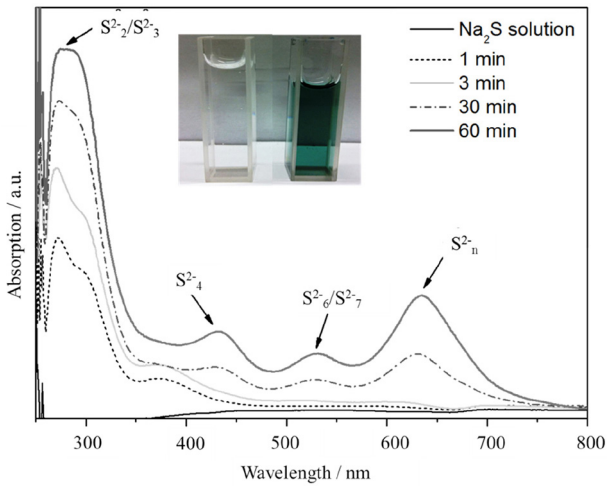

Figure 8. UV-Vis spectra evolution during the sulfide oxidation in the presence of $MW_{600}1$ (UV-Vis spectra for the other catalysts not shown).

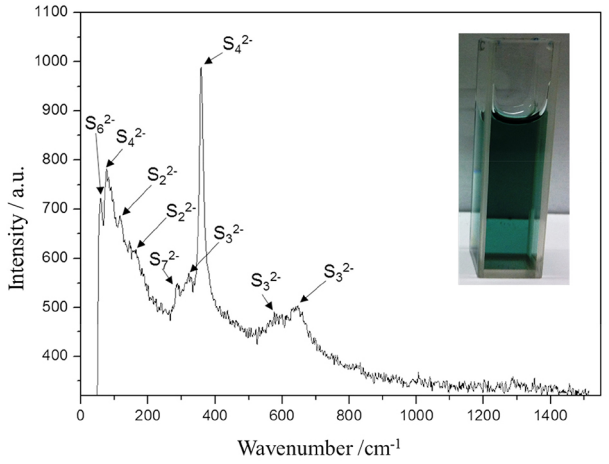

Figure 9. Raman spectrum obtained for the solution from after sulfide oxidation.

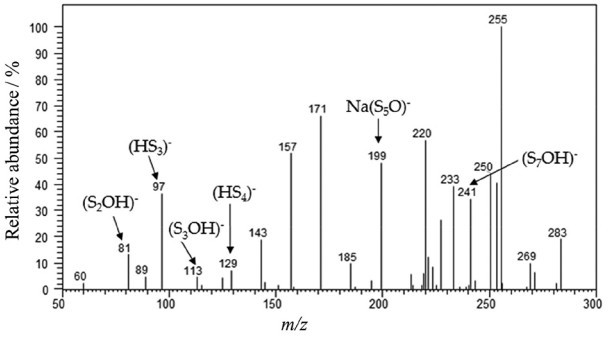

Figure 10. Mass spectrum of the resulting solution of the reaction between the composite $MW_{600}1$ and sodium sulfide solution obtained in negative mode of PS-MS.

These results corroborate the UV-Vis and Raman spectra with the presence of ions with 2 to 7 sulfur atoms compounds. In addition, different oxidized polysulfides species were observed associated with Na^+. Additional optimizations are under investigation, aiming to obtain best conditions for data acquisition and ion's identification.

UV monitoring of the most intense band at 270 nm related to the first specie formed S_2^{2-} was used to investigate the kinetic and catalysts efficiency. Figure 11 shows that pure magnetite does not have a significant activity for sulfide oxidation.

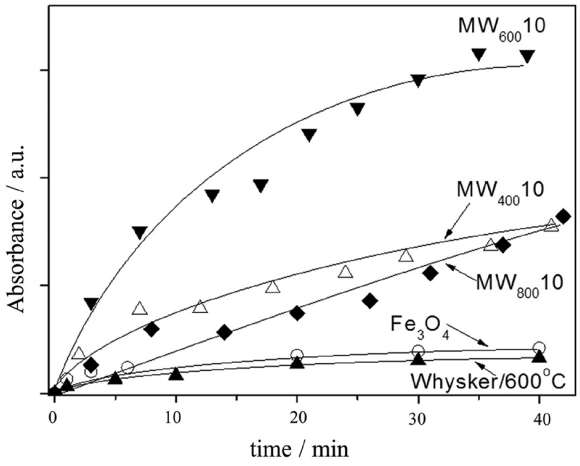

Figure 11. Sulfide oxidation monitored by the band at 270 nm with the catalysts treated at different temperatures.

It can also be observed that the pure carbon obtained by pyrolysis of the cellulose nanocrystals (without Fe_3O_4) at 600 °C showed a very low catalytic activity. On the other hand, the use of the composites based on Fe_3O_4 with 10% carbon showed much higher activities. Treatment at 400 °C ($MW_{400}10$) produced a significant increase in the activity for sulfide oxidation. However, treatment at 600 °C showed a remarkable increase on the sulfide oxidation whereas at 800 °C a strong loss of activity was observed.

The effect of the carbon content was investigated for the series obtained at 600 °C, i.e., $MW_{600}1$, $MW_{600}10$ and $MW_{600}20$ (Figure 12).

It can be observed again that all the composites are more active than the pure Fe_3O_4 and pure carbon obtained at 600 °C. As the carbon content increased from 1 to 10% the oxidation activity strongly increased. On the other hand, when the carbon content increased from 10 to 20% a strong decrease in the catalytic activity was observed, likely due to an extensive coating and even encapsulation of the Fe_3O_4 particles as it was observed by SEM.

It was monitored the UV-Vis band intensities for the different S_n^{2-} species (see Supplementary Information section). It was observed that the species S_2^{2-} and S_3^{2-} with higher intensities gradually increased and tending to remain constant after 30 min of reaction. The specie S_4^{2-} with a less intense absorption showed similar behavior.

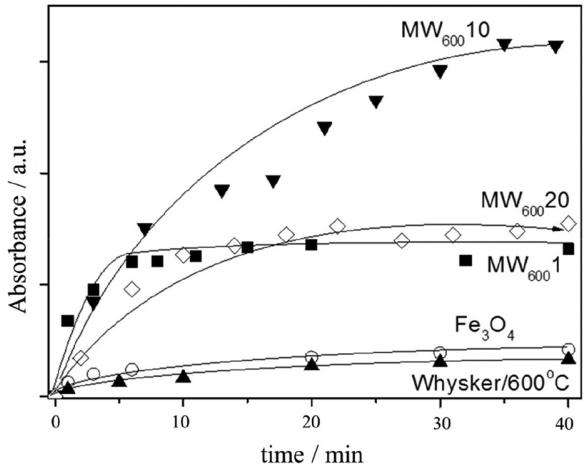

Figure 12. Sulfide oxidation monitored by the band at 270 nm with the catalysts with different carbon contents.

The higher polysulfides together showed a continuous increase in intensity. These results do not indicate that the polysulfides are formed sequentially, e.g., S_3^{2-} is formed from S_2^{2-}. Apparently, these polysulfides are formed simultaneously on the catalyst surface and once released to the surface they are not converted significantly to the higher polysulfides.

These results clearly showed that the composite combining carbon and Fe_3O_4, especially $MW_{600}10$, is much more active for sulfide oxidation compared to the isolated phases.

Although the nature of this higher activity is not clear, previous works indicated that for the sulfide oxidation two features are very important in the catalyst, i.e., the presence of surface redox groups and electron transfer properties.[9,10] The high activity observed for carbon based materials, i.e., activated carbon, graphite and graphene,[9,10] was related to the presence of redox groups, e.g., quinone, that can easily oxidize sulfide. Moreover, it was also suggested that the electron conductivity was important for the sulfide oxidation activity. These effects of redox surface groups and electron conductivity were also discussed in recent work on ferrites (MFe_2O_4 where M = Co, Cu) as catalyst for sulfide oxidation.[18]

The higher activity observed for the composite $MW_{600}10$ could be related to a synergic combination of the properties of carbon and magnetite, which are described below.

The carbon surface obtained at 600 °C should have oxygen based redox groups, e.g., quinone, since these groups have been observed in previous work and indicated by FTIR and potentiometric titration in this work. These redox groups can be reduced by sulfide according to a simplified reaction, equation 3.

$$\text{Carbon}{-}\text{C}{=}\text{O}_{surf} + \text{S}^{2-}{}_{aq} \rightarrow \text{Carbon}{-}\text{C}{-}\text{O}^{-}/\text{S}^{-}{}_{surf} \quad (3)$$

These reduced groups, e.g., hydroquinones, should transfer electrons to regenerate and continue the catalytic cycle. One possible pathway is to transfer these electrons to magnetite, which can be easily accommodated by structural Fe^{3+} species producing Fe^{2+}, equation 4.

$$(Fe^{2+})\,(Fe^{3+})_2O_4 + e^- \rightarrow (Fe^{2+})_{1+x}\,(Fe^{3+})_{2-x}O_4 \quad (4)$$

Considering this electron transfer process, the interface carbon/Fe_3O_4 is very important for the reaction. Although there is no direct evidence of the carbon/Fe_3O_4 interface, the data shown in this work suggest that after the cellulose decomposition, the carbon formed will react with the Fe_3O_4 surface at 600 °C likely to form an interface.

After the electron is transferred to magnetite, the Fe^{2+} species produced should then transfer those electrons to the reaction medium. Although the destination of these electrons is not clear, some possible reactions are the reduction of H_2O or O_2 which are well known to take place by Fe^{2+} present in the oxide structures (equations 5 and 6).[45-48]

$$2\,H_2O + 2e^- \rightarrow H_2 + 2\,OH^- \quad (5)$$

$$½\,O_2 + H_2O + 2\,e^- \rightarrow 2\,OH^- \quad (6)$$

It is interesting to observe that the composite treated at 800 °C showed low activity for sulfide oxidation. This decrease on the activity is likely due to the conversion of the Fe_3O_4 to the metallic phase and also to the decomposition of the oxygen surface groups present in the carbon structure (see FTIR and titration data on Table S1 in Supplementary Information section).

A hypothetical mechanism taking into account all these effects can be proposed (Figure 13).

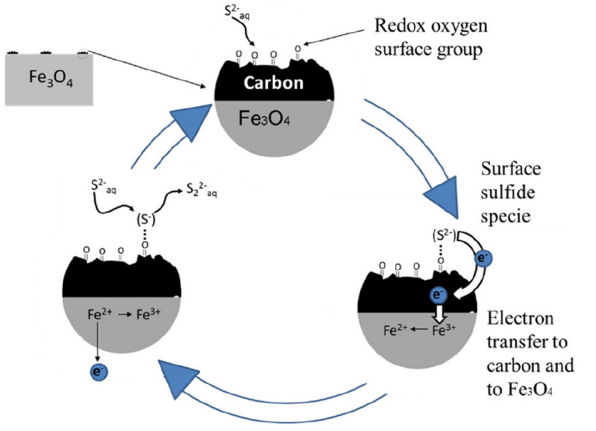

Figure 13. Schematic representation of a mechanism proposal for the electron transfer through the composites.

In this mechanism, the sulfide reacts with oxygen redox groups on the carbon surface and the electrons are transferred

via an interface to the magnetite structure reducing a Fe^{3+} species to Fe^{2+}. Details of the reaction mechanism are under investigation using X-ray photoelectron spectroscopy (XPS), cyclic voltammetry and electron paramagnetic resonance (EPR) measurements in different systems based on graphene and carbon nanotubes with iron oxides films.

Conclusions

Cellulose nanocrystal can be combined by assembling cellulose nanocrystals surrounding Fe_3O_4 followed by a controlled thermal decomposition. The obtained results indicated that at 400 and 600 °C the cellulose nanocrystals decompose to form carbon films, filaments and particles attached to the Fe_3O_4 crystals. These C interfaced with Fe_3O_4 composites catalyze the oxidation of aqueous sulfide to convert S^{2-}_{aq} to polysulfides S_n^{2-} (where n = 2-9) and also oxygen containing polysulfides HOS_n^-. Simple kinetic experiments showed that the composites, especially with 10% C obtained at 600 °C, were remarkably active. Although the nature of this synergic effect is not clear, a possible operational mechanism involves the participation of oxygen based redox groups present on the carbon surface and an electron transfer from the carbon to the Fe_3O_4 phase. Moreover, these magnetic materials can be easily separated from the reaction medium by a simple magnetic process, which is a very interesting technological advantage.

Supplementary Information

The Supplementary Information (hyperfine parameters, Raman spectra and thermal decomposition of the catalysts) is available free of charge at http://jbcs.sbq.org.br as a PDF file.

Acknowledgements

The authors acknowledge the support of Petrobras, FAPEMIG, PRPq/UFMG, CNPq and CAPES. Thanks for the SEM/EDS provided by the UFMG Microscopy Center.

References

1. Burgess, J. E.; Parsons, S. A.; Stuetz, R. M.; *Biotechnol. Adv.* **2001**, *19*, 35.
2. Tchobanoglous, G.; Burton, F. L.; Stensel, H. D.; *Wastewater Engineering: Treatment and Reuse*; McGraw-Hill Science/ Engineering/Math: New York, 2003.
3. Llansó, R. J.; *J. Exp. Mar. Biol. Ecol.* **1991**, *153*, 165.
4. Wiener, M. S.; Salas, B. V.; Quintero-Núñez, M.; Zlatev, R.; *Corros. Eng., Sci. Technol.* **2006**, *41*, 221.
5. Zhang, L.; de Schryver, P.; de Gusseme, B.; de Muynck, W.; Boon, N.; Verstraete, W.; *Water Res.* **2008**, *42*, 1.
6. León, M.; Jiménez-Jiménez, J.; Jiménez-López, A.; Rodríguez-Castellón, E.; Soriano, D.; López Nieto, J. M.; *Solid State Sci.* **2010**, *12*, 996.
7. Kapse, V. D.; Ghosh, S. A.; Raghuwanshi, F. C.; Kapse, S. D.; *Mater. Chem. Phys.* **2009**, *113*, 638.
8. Jeyakumar, K.; Chakravarthy, R. D.; Chand, D. K.; *Catal. Commun.* **2009**, *10*, 1948.
9. Lemos, B. R. S.; Teixeira, I. F.; de Mesquita, J. P.; Ribeiro, R. R.; Donnici, C. L.; Lago, R. M.; *Carbon* **2012**, *50*, 1386.
10. Lemos, B. R. S.; Teixeira, I. F.; Machado, B. F.; Alves, M. R. A.; de Mesquita, J. P.; Ribeiro, R. R.; Bacsa, R. R.; Serp, P.; Lago, R. M.; *J. Mater. Chem. A* **2013**, *1*, 9491.
11. Vairavamurthy, A.; Manowitz, B.; Zhou, W. Q.; Jeon, Y. S. In *Environmental Geochemistry of Sulfide Oxidation (Determination of Hydrogen-Sulfide Oxidation-Products by Sulfur K-Edge X-ray-Absorption Near-Edge Structure spectroscopy)*; Alpers, C. N.; Blowes, D. W., eds.; Wiley-VCH: Weinheim, Germany, 1994, ch. 7, pp. 412.
12. Hoffmann, M. R.; Lim, B. C.; *Environ. Sci. Technol.* **1979**, *13*, 1406.
13. Weres, O.; Tsao, L.; Chhatre, R. M.; *Corrosion* **1985**, *41*, 307.
14. Macy, J.; Schröder, I.; Thauer, R.; Kröger, A.; *Arch. Microbiol.* **1986**, *144*, 147.
15. Henshaw, P. F.; Zhu, W.; *Water Res.* **2001**, *35*, 3605.
16. Friedrich, C. G.; Rother, D.; Bardischewsky, F.; Quentmeier, A.; Fischer, J.; *Appl. Environ. Microbiol.* **2001**, *67*, 2873.
17. Schutz, M.; Klughammer, C.; Griesbeck, C.; Quentmeier, A.; Friedrich, C. G.; Hauska, G.; *Arch. Microbiol.* **1998**, *170*, 353.
18. Cunha, I. T.; Teixeira, I. F.; Albuquerque, A. S.; Ardisson, J. D.; Macedo, W. A. A.; Oliveira, H. S.; Tristao, J. C.; Sapag, K.; Lago, R. M.; *Catal. Today*, *in press*, DOI: 10.1016/j.cattod.2015.07.023.
19. de Rodriguez, N. L. G.; Thielemans, W.; Dufresne, A.; *Cellulose* **2006**, *13*, 261.
20. Brito, B. L.; Pereira, F.; Putaux, J.-L.; Jean, B.; *Cellulose* **2012**, *19*, 1527.
21. de Mesquita, J. P.; Reis, L. S.; Purceno, A. D.; Donnici, C. L.; Lago, R. M.; Pereira, F. V.; *J. Chem. Technol. Biotechnol.* **2013**, *88*, 1130.
22. Shebanova, O. N.; Lazor, P.; *J. Raman Spectrosc.* **2003**, *34*, 845.
23. Kundu, S.; Wang, Y.; Xia, W.; Muhler, M.; *J. Phys. Chem. C* **2008**, *112*, 16869.
24. Haydar, S.; Moreno-Castilla, C.; Ferro-García, M. A.; Carrasco-Marín, F.; Rivera-Utrilla, J.; Perrard, A.; Joly, J. P.; *Carbon* **2000**, *38*, 1297.
25. Gorgulho, H. F.; Mesquita, J. P.; Gonçalves, F.; Pereira, M. F. R.; Figueiredo, J. L.; *Carbon* **2008**, *46*, 1544.
26. de Mesquita, J. P.; Martelli, P. B.; Gorgulho, H. D. F.; *J. Braz. Chem. Soc.* **2006**, *17*, 1133.

27. Teixeira, I. F.; Medeiros, T. P. V.; Freitas, P. E.; Rosmaninho, M. G.; Ardisson, J. D.; Lago, R. M.; *Fuel* **2014**, *124*, 7.
28. Pereira, M. C.; Coelho, F. S.; Nascentes, C. C.; Fabris, J. D.; Araújo, M. H.; Sapag, K.; Oliveira, L. C. A.; Lago, R. M.; *Chemosphere* **2010**, *81*, 7.
29. Amorim, C. C.; Leão, M. M. D.; Dutra, P. R.; Tristão, J. C.; Magalhães, F.; Lago, R. M.; *Chemosphere* **2014**, *109*, 143.
30. Karimi, E.; Teixeira, I. F.; Gomez, A.; de Resende, E.; Gissane, C.; Leitch, J.; Jollet, V.; Aigner, I.; Berruti, F.; Briens, C.; Fransham, P.; Hoff, B.; Schrier, N.; Lago, R. M.; Kycia, S. W.; Heck, R.; Schlaf, M.; *Appl. Catal., B* **2014**, *145*, 187.
31. Oliveira, P. E. F.; Ribeiro, L. P.; Rosmaninho, M. G.; Ardisson, J. D.; Dias, A.; Oliveira, L. C. A.; Lago, R. M.; *Catal. Commun.* **2013**, *32*, 58.
32. Amorim, C. C.; Dutra, P. R.; Leão, M. M. D.; Pereira, M. C.; Henriques, A. B.; Fabris, J. D.; Lago, R. M.; *Chem. Eng. J.* **2012**, *209*, 645.
33. Rosmaninho, M. G.; Moura, F. C. C.; Souza, L. R.; Nogueira, R. K.; Gomes, G. M.; Nascimento, J. S.; Pereira, M. C.; Fabris, J. D.; Ardisson, J. D.; Nazzarro, M. S.; Sapag, K.; Araújo, M. H.; Lago, R. M.; *Appl. Catal., B* **2012**, *115-116*, 45.
34. Teixeira, A. P. C.; Tristao, J. C.; Araujo, M. H.; Oliveira, L. C. A.; Moura, F. C. C.; Ardisson, J. D.; Amorim, C. C.; Lago, R. M.; *J. Braz. Chem. Soc.* **2012**, *23*, 1579.
35. Linkous, C. A.; Huang, C.; Fowler, J. R.; *J. Photochem. Photobiol., A* **2004**, *168*, 153.
36. Steudel, R.; Holdt, G.; Gobel, T.; *J. Chromatogr.* **1989**, *475*, 442.
37. Fleet, M. E.; Liu, X.; *Spectrochim. Acta, Part B* **2010**, *65*, 75.
38. Scheers, J.; Fantini, S.; Johansson, P.; *J. Power Sources* **2014**, *255*, 204.
39. Müller, A.; Krebs, B.; *Sulfur: Its Significance for Chemistry, for the Geo-, Bio-, and Cosmosphere and Technology*; Elsevier Science: Amsterdam, 2013.
40. Janz, G. J.; Downey, J. R.; Roduner, E.; Wasilczyk, G. J.; Coutts, J. W.; Eluard, A.; *Inorg. Chem.* **1976**, *15*, 1759.
41. el Jaroudi, O.; Picquenard, E.; Gobeltz, N.; Demortier, A.; Corset, J.; *Inorg. Chem.* **1999**, *38*, 2917.
42. Steudel, R. In *Elemental Sulfur und Sulfur-Rich Compounds II (Inorganic Polysulfanes H_2S n with n > 1)*; Steudel, R., ed.; Springer Berlin Heidelberg: Berlin, 2003.
43. Trofimov, B. A.; Sinegovskaya, L. M.; Gusarova, N. K.; *J. Sulfur Chem.* **2009**, *30*, 518.
44. Gun, J.; Modestov, A. D.; Kamyshny Jr., A.; Ryzkov, D.; Gitis, V.; Goifman, A.; Lev, O.; Hultsch, V.; Grischek, T.; Worch, E.; *Microchim. Acta* **2004**, *146*, 229.
45. Nippe, M.; Khnayzer, R. S.; Panetier, J. A.; Zee, D. Z.; Olaiya, B. S.; Head-Gordon, M.; Chang, C. J.; Castellano, F. N.; Long, J. R.; *Chem. Sci.* **2013**, *4*, 3934.
46. Navarro-Solís, I.; Villalba-Almendra, L.; Alvarez-Gallegos, A.; *Int. J. Hydrogen Energy* **2010**, *35*, 10833.
47. Nemes, Á.; Inzelt, G.; *J. Solid State Electrochem.* **2014**, *18*, 3327.
48. Zhang, J.; Wang, X.; Qin, D.; Xue, Z.; Lu, X.; *Appl. Surf. Sci.* **2014**, *320*, 73.

Submitted: August 10, 2015
Published online: October 27, 2015